Journal of Materials Science: Materials in Electronics (2019) 30:7808–7814
https://doi.org/10.1007/s10854-019-01097-3

$Ca_2ZrSi_4O_{12}:Eu^{3+}$, Bi^{3+} phosphor: synthesis, tunable emission, and luminescence properties

Renping Cao[1] · Lei Su[1] · Xinyu Cheng[1] · Ting Chen[1] · Chenxing Liao[2] · Yimin Guo[1] · Pan Liu[1] · Wensheng Li[1]

Received: 31 December 2018 / Accepted: 7 March 2019 / Published online: 12 March 2019

Abstract
$Ca_2ZrSi_4O_{12}$:R (CZSO:R) (R = Eu^{3+}, Bi^{3+}, and Eu^{3+}/Bi^{3+}) phosphors are successfully synthesized in air through high-temperature solid-state method. Host CZSO and CZSO:Bi^{3+} phosphor with excitation at 300 nm emit blue light. CZSO:Eu^{3+} phosphor with changing Eu^{3+} content shows tunable emission from white to red light under excitation at 300 nm and only emits red light under excitation at 395 nm. CZSO:10%Eu^{3+}, Bi^{3+} phosphor shows tunable emission from blue to red light under excitation at 300 nm, and only emits red light with excitation at 395 nm when Bi^{3+} ion concentration is changed. Luminescence properties of CZSO:Eu^{3+} phosphor may be improved by co-doping Bi^{3+} ion. The luminous mechanism of CZSO:Eu^{3+}, Bi^{3+} phosphor is explained by the energy level diagrams of Bi^{3+} and Eu^{3+} ions.

1 Introduction

The luminescent materials play an important role in modern lighting and display fields due to their abundant emission properties [1]. Rare earth and main-group metal ions as the important activators in luminescent materials have been researched and reported widely [2–4]. Eu^{3+} ion as one of rare earth ions has been known as an excellent activator in many luminescent materials [5–7]. Eu^{3+}-doped luminescent materials usually show red emission and their emission spectra are observed in the range of 580–725 nm with excitation at ultraviolet (UV) and near UV light due to the $^5D_0 \rightarrow {}^7F_J$ (J = 0, 1, 2, 3, 4) transitions of Eu^{3+} ion [8, 9]. The excitation spectra of Eu^{3+}-doped luminescent materials cover the region from 220 nm to 550 nm owing to the *f–f* transitions of Eu^{3+} ion. However, Eu^{3+}-doped luminescent materials have the weak absorption bands in the range of 400–550 nm, so, it is very meaningful to improve this weakness. Bi^{3+}-doped luminescent materials with excitation at UV light can show a series of different emissions from blue to orange-red light and their emission spectra cover the region from 400 to 750 nm due to the $^3P_{0,1} \rightarrow {}^1S_0$ transitions and the metal-to-metal charge-transfer (MMCT) [10–12]. An interesting phenomenon may be found that the emission spectra of Bi^{3+}-doped luminescent materials have an overlap with the excitation spectra of Eu^{3+}-doped luminescent materials in the range of 400–550 nm. That is to say. When Eu^{3+} and Bi^{3+} ions are codoped into the same host materials, energy transfer (ET) may be formed from Bi^{3+} to Eu^{3+} ions, which is helpful for the luminescence property improvement of Eu^{3+}-doped luminescent materials [13, 14]. At the same time, it should be noted that host material is also one of the most important factors affecting the luminescence property of luminescent materials.

Materials containing the O^{2-}–Zr^{4+} charge transfer (CT) have been used as host for rare earth ions [15, 16]. This host materials have a broad absorption band due to the O^{2-}–Zr^{4+} CT and show a broadband emission. This optical property of host materials may be used to improve the luminescence properties of rare earth ion as activator. $Ca_2ZrSi_4O_{12}$ has many advantages, such as the good thermal stability, low dielectric constant, and relatively high quality factor [17]. $Ca_2ZrSi_4O_{12}$ can show intense emission because of the $Zr^{4+} \rightarrow O^{2-}$ transition [18]. Up to now, $Ca_2ZrSi_4O_{12}$:R (CZSO:R) (R = Eu^{3+}, Eu^{3+}/Bi^{3+}) phosphors have not been reported. Therefore, we choose $Ca_2ZrSi_4O_{12}$ as host material to study the influence of ET process to the luminescence properties.

In this work, we synthesize CZSO:Eu^{3+}, CZSO:Bi^{3+}, and CZSO:Eu^{3+}, Bi^{3+} phosphors in air through high-temperature

✉ Renping Cao
jxcrp@163.com

[1] College of Mathematics and Physics, Jinggangshan University, Ji'an 343009, People's Republic of China

[2] School of Materials Science and Engineering, University of Science and Technology, Ganzhou 341000, Jiangxi, People's Republic of China

solid-state method, and investigate their crystal structures, decay curves, and luminescence properties. The influences of activator (Eu^{3+} or Bi^{3+}) concentration to luminescence properties are discussed. ET from host and Bi^{3+} ion to Eu^{3+} ion is observed. The luminous mechanism is explained by energy level diagrams of Eu^{3+} and Bi^{3+} ions.

2 Experimental

2.1 Synthesis process

CZSO:xEu^{3+} (x = 0, 2, 4, 6, 8, 10, and 12 mol%), CZSO:6%Bi^{3+}, and CZSO:10%Eu^{3+}, yBi^{3+} (y = 2, 4, 6, 8, and 10 mol%) phosphors are synthesized in air through high-temperature solid-state method with the raw materials (e.g., $CaCO_3$ (A.R. 99.9%), ZrO_2 (A.R. 99.9%), SiO_2 (A.R. 99.9%), Eu_2O_3 (99.99%), and Bi_2O_3 (99.99%)). The raw materials are weighted in stoichiometric ratios according to the chemical formula and throughly ground for 20 min by using an agate mortar in order to form homogeneous mixture. Then, the mixtures are put into an alumina crucible, loaded into a muffle furnace, and sintered at 700 °C for 6 h. After the mixtures are cooled to room temperature, they are reground for 15 min. The mixtures are placed in the muffle furnace to be calcined again. To complete the chemical reaction, the sintering temperature and time are 1300 °C and 6 h, respectively. Finally, the samples are cooled to room temperature within the furnace and then reground by using an agate mortar for the properties characterization.

2.2 Characterization

The crystal structures and phases of samples are researched by X-ray powder diffractions (XRD) diffractometer (Philips Model PW1830) with a graphite monochromator by using Cu-Kα radiation at 40 mA, 40 kV and scanning step of 0.02°. The scanning region of 2θ angle is from 10° to 75°. The decay curves, quantum efficiency (QE), and luminescence properties are recorded by using a FLS-980 spectrophotometer (Edinburgh Instruments Ltd, Edinburgh, U.K.) for steady-state spectrum measurement. The excitation source is the 450 W ozone free xenon lamp. A microsecond pulsed xenon flash lamp μF900 is available to record the decay curves for lifetimes with an average power of 60 W.

3 Results and discussion

The crystal structure of CZSO drawn on the strength of the Inorganic Crystal Structure Database (ICSD) #73,801 is displayed in Fig. 1. The cell of host CZSO is a monoclinic system with space-group $P2_1/m$ and the lattice parameters (a = 7.399(1) Å, b = 13.651(2) Å, c = 5.312(1) Å, β = 108.9(2)°, V = 507.60(62) $Å^3$, and Z = 2) [17]. Ca^{2+}/Si^{4+} and Zr^{4+} ions have two and one crystallographic sites, respectively. Ca atom has 8- and 9- coordination ([CaO_8] and [CaO_9]). Si atom with four O atoms is formed [SiO_4] tetrahedron. Zr atom is coordinated by six oxygen atoms and forms a [ZrO_6] octahedron. In host CZSO, the ionic radii of the cations are (Ca^{2+}: CN = 8, 1.12 Å and CN = 9, 1.18 Å, Zr^{4+}: CN = 6, 0.72 Å, and Si^{4+}: CN = 4, 0.262 Å) [19]. The ionic radii of the activators are (Eu^{3+}: CN = 8, 1.07 Å and CN = 9, 1.12 Å, Bi^{3+}: CN = 8, 1.17 Å) [19]. According to the ionic radius similarity mechanism, Eu^{3+} and Bi^{3+} ions can replace the Ca^{2+} sites in host CZSO lattice. In order to keep the charge balance of host CZSO lattice, the electron hole (v^-) may be occured and the charge balanced relation is (Eu^{3+} or $Bi^{3+} \rightarrow Ca^{2+} + v^-$).

XRD patterns of the Joint Committee Powder Diffraction Standard (JCPDS) no. 81-2342 (CZSO), CZSO:xEu^{3+} (x = 0, 4, and 10 mol%), and CZSO:10%Eu^{3+}, yBi^{3+} (y = 4 and 10 mol%) phosphors in the 2θ range of 10°–75° are presented in Fig. 2. It can be clearly observed that XRD patterns of the samples are well consistent with that of JCPDS no. 81-2342 (CZSO) and there are not other XRD pattern peaks derived from impurities and raw materials. That is to say, there is only a single phase (CZSO) in these samples.

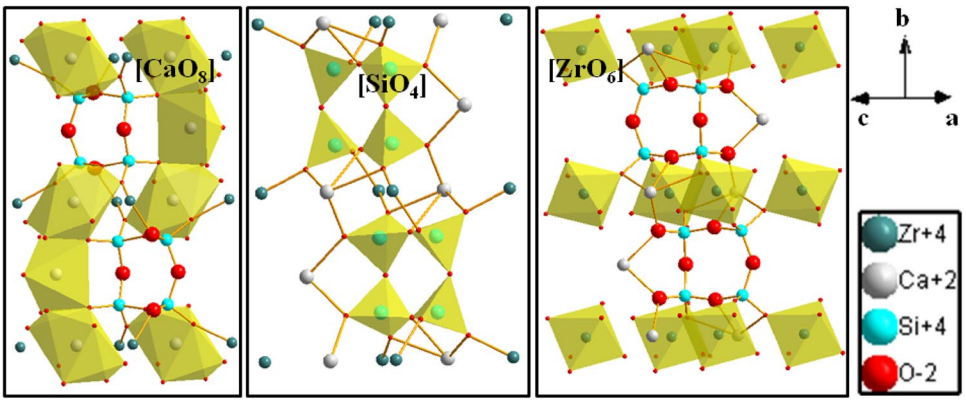

Fig. 1 The crystal structure of CZSO drawn on the strength of ICSD #73801

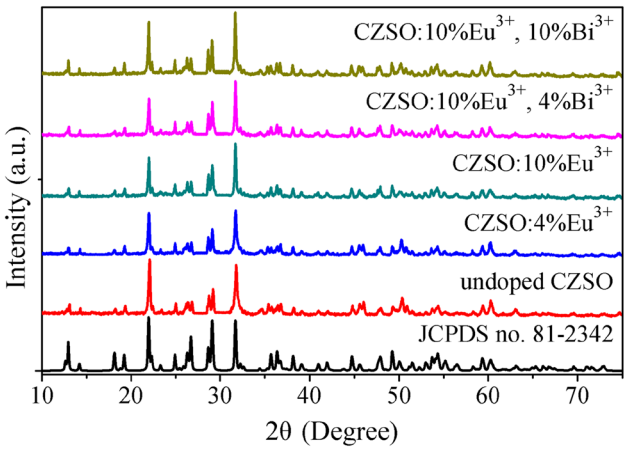

Fig. 2 XRD patterns of JCPDS no. 81-2342 (CZSO), CZSO:xEu^{3+} (x = 0, 4, and 10 mol%), and CZSO:10%Eu^{3+}, yBi^{3+} (y = 4 and 10 mol%) phosphors in the 2θ range of 10°–75°

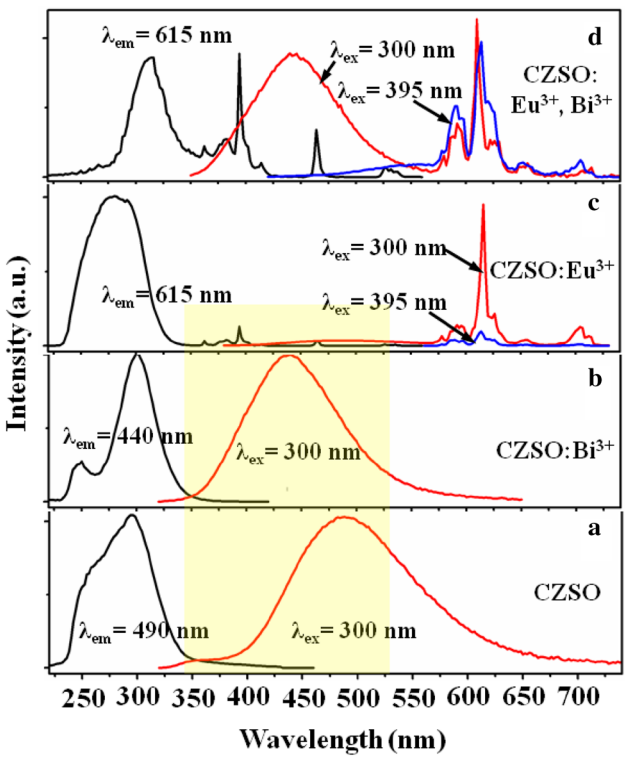

Fig. 3 PLE and PL spectra of **a** host CZSO (λ_{ex} = 300 nm and λ_{em} = 490 nm), **b** CZSO:6%Bi^{3+} (λ_{ex} = 300 nm and λ_{em} = 440 nm), **c** CZSO:10%Eu^{3+} (λ_{ex} = 300 and 395 nm; λ_{em} = 615 nm), and **d** CZSO:10%Eu^{3+}, 6%Bi^{3+} (λ_{ex} = 300 and 395 nm; λ_{em} = 615 nm) phosphors at room temperature

The experimental result makes clear that these samples are successfully synthesized and the crystal structure of host CZSO is not led to the significant changes because of the doping of Eu^{3+} and Bi^{3+} ions.

Photoluminescence excitation (PLE) and photoluminescence (PL) spectra of host CZSO at room temperature are shown in Fig. 3a. Monitored at 490 nm, a PLE band peaking at ~ 300 nm of host CZSO can be observed in the range of 230–350 nm because of the O^{2-}–Zr^{4+} CT inside [ZrO_6] group [20]. With excitation at 300 nm, a broad PL band peaking at ~ 490 nnm and a weak PL band peaking at ~ 355 nm of host CZSO are shown in the rang of 325–700 nm due to the $Zr^{4+} \rightarrow O^{2-}$ transition [21]. PLE and PL spectra of CZSO:6%Bi^{3+} phosphor at room temperature are presented in Fig. 3b. It can be found that emission derived from host CZSO is not observed after Bi^{3+} ion is doped. Monitored at 440 nm, PLE band of CZSO:6%Bi^{3+} phosphor containing two PLE peaks is observed in the range of 230–350 nm, which are attributed to the $^1S_0 \rightarrow {}^1P_1$ transition of Bi^{3+} ion (~ 250 nm), and the $^1S_0 \rightarrow {}^3P_1$ transition of Bi^{3+} ion and $Bi^{3+} \rightarrow Zr^{4+}$ MMCT (~ 300 nm), respectively [22, 23]. CZSO:6%Bi^{3+} phosphor with excitation at 300 nm shows a broadband emission with PL peak at ~ 440 nm in the range of 350–650 nm, which is assigned to the $Zr^{4+} \rightarrow Bi^{3+}$ transition and the $^3P_1 \rightarrow {}^1S_0$ transition of Bi^{3+} ion [24, 25].

PLE and PL spectra of CZSO:10%Eu^{3+} phosphor at room temperature are shown in Fig. 3c. PLE spectrum of CZSO:10%Eu^{3+} phosphor monitored at 615 nm can be observed in the range of 230–550 nm, which includes a broad PLE band and five narrow PLE bands. The broad PLE band in the range of 230–350 nm is assigned to the O^{2-}–Eu^{3+} and O^{2-}–Zr^{4+} CTs, and the narrow PLE bands in the range of 350–550 nm are attributed to the 4*f*–4*f* transitions of Eu^{3+} ion [26, 27]. The strongest characteristic peak (395 nm) of Eu^{3+} ion is attributed to the $^7F_0 \rightarrow {}^5L_6$ transition of Eu^{3+} ion. With excitation at 300 nm, PL spectrum of CZSO:10%Eu^{3+} phosphor in the range of 380–725 nm can be observed, which contains a weak broad PL band derived from host CZSO and four narrow PL bands owing to the $^5D_0 \rightarrow {}^7F_1$, $^7F_2$, $^7F_3$, and $^7F_4$ transitions of Eu^{3+} ion [28, 29]. With excitation at 395 nm, the emission of host CZSO is not observed because it does not have the absorption band at 395 nm, thus, CZSO:10%Eu^{3+} phosphor only shows the emission of Eu^{3+} ion in the range of 560–725 nm. According to the spectral properties in Fig. 3a–c, there is a very interesting phenomenon that the PL spectra of host CZSO and CZSO:Bi^{3+} phosphor with excitation at 300 nm have an overlap with PLE spectrum of CZSO:10%Eu^{3+} phosphor in the range of 350–550 nm, causing ET from host CZSO and Bi^{3+} ion to Eu^{3+} ion. The ET phenomenon from Bi^{3+} to Eu^{3+} ions in other phosphors has also been reported, such as $SrSb_2O_6$:Eu^{3+}, Bi^{3+} [30], SrY_2O_4:Bi^{3+},Eu^{3+} [31], and $Ba_9Y_2Si_6O_{24}$:Eu^{3+}, Bi^{3+} [32].

PLE and PL spectra of CZSO:10%Eu^{3+}, 6%Bi^{3+} phosphor at room temperature are displayed in Fig. 3d. Monitored at 615 nm, PLE spectrum of CZSO:10%Eu^{3+}, 6%Bi^{3+} phosphor contains the PLE bands derived from Bi^{3+} and

Eu^{3+} ions in the range of 230–550 nm. With excitation at 300 nm, PL spectrum of CZSO:10%Eu^{3+}, 6%Bi^{3+} phosphor in the range of 350–725 nm can be observed, which includes the PL bands derived from Bi^{3+} and Eu^{3+} ions. With excitation at 395 nm, the emissions of host CZSO and Bi^{3+} ion are not observed because they do not have the absorption band at 395 nm, thus, CZSO:10%Eu^{3+}, 6%Bi^{3+} phosphor only shows the emission derived from Eu^{3+} ion in the range of 560–725 nm. Moreover, we measure the QE of CZSO:10%Eu^{3+} and CZSO:10%Eu^{3+}, 6%Bi^{3+} phosphors monitored at 615 with excitation at 300 nm by FLS-980 spectrophotometer with integrating sphere. The QE of CZSO:10%Eu^{3+} and CZSO:10%Eu^{3+}, 6%Bi^{3+} phosphors are found to be 35.5% and 42.3%, respectively, indicating that the co-doping Bi^{3+} ion is helpful to improve the, luminescence properties of CZSO:10%Eu^{3+} phosphor.

The simple description diagram of the luminescence mechanism of CZSO:Eu^{3+}, Bi^{3+} phosphor by energy level diagrams of Bi^{3+} and Eu^{3+} ions and the ET process are shown in Fig. 4. In host CZSO, under UV excitation, the electrons in the valence band are excited to the conductive band, part of electron energy may be transferred to the emission center (Eu^{3+}) by ET, and the other part energy is released via the emission. In Bi^{3+} ion, there are a ground state $^1S_0$ and four excited states $^3P_{0,1,2}$ and $^1P_1$. Here, with excitation at UV light, free electrons absorb energy and are raised to excited states $^3P_1$ and $^1P_1$ from ground state $^1S_0$ [33]. Part of electron energy may be transferred to the emission center (Eu^{3+}) by ET and the other part energy is released by the $^3P_1 \rightarrow {}^1S_0$ transition, resulting in the emission. After free electrons in Eu^{3+} ion absorb the energy derived from UV excitation, host CZSO, and Bi^{3+} ion, they are raised to high excited states from ground state $^7F_0$ by the 4*f*–4*f* transition. Those electrons at high excited states return to low excited states by non-radiative, locate at the excited states $^5D_0$, and finally come back to the ground states by the $^5D_0 \rightarrow {}^7F_1$, $^7F_2$, $^7F_3$, and $^7F_4$ transitions of Eu^{3+} ion, releasing photon energy through emission [34].

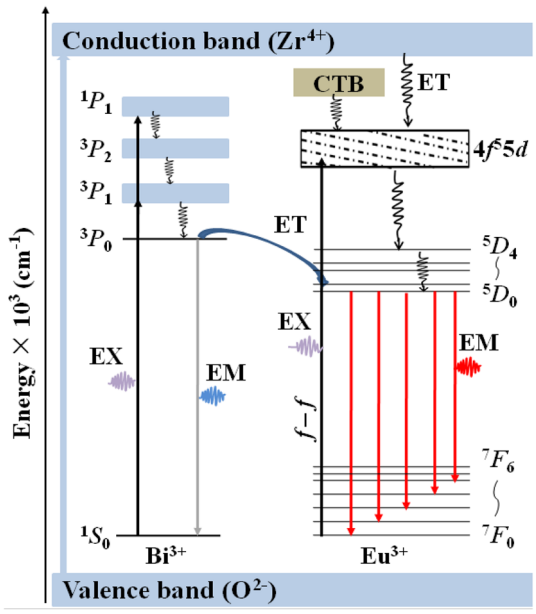

Fig. 4 The simple description diagram of the luminescence mechanism of CZSO:Eu^{3+}, Bi^{3+} phosphor by energy level diagrams of Bi^{3+} and Eu^{3+} ions and the ET process

The room temperature PL spectra of CZSO:xEu^{3+} (x = 2, 4, 6, 8, 10, and 12 mol%) phosphors with excitation at 300 nm, the corresponding Commission Internationale de l'Eclairage (CIE) chromaticity diagrams and chromaticity coordinates are shown in Fig. 5a. It can be found that the emission intensity of CZSO:Eu^{3+} phosphor is the strongest when x = 10 mol%, and a tunable emission of CZSO:Eu^{3+} phosphor from white to red light may be observed with changing Eu^{3+} concentration, which is shown in the corresponding CIE chromaticity diagram. The chromaticity coordinates of CZSO:Eu^{3+} phosphor with excitation at 300 nm are changed from (0.3061, 0.3165) to (0.5323, 0.3717) with increasing Eu^{3+} concentration from 2 mol% to 12 mol%, which are shown in Table 1.

The room temperature PL spectra of CZSO:xEu^{3+} (x = 2, 4, 6, 8, 10, and 12 mol%) phosphors with excitation at 395 nm, the corresponding CIE chromaticity diagrams and chromaticity coordinates, and the relation between Eu^{3+} ion concentration and PL intensity are presented in Fig. 5b. When x < 10 mol%, PL intensity of CZSO:Eu^{3+} phosphor increases with increasing Eu^{3+} ion concentration from 2 mol% to 10 mol% because of ET that is derived from host CZSO and among Eu^{3+} ion. The PL intensity of CZSO:Eu^{3+} phosphor is the strongest when x = 10 mol%, then decreases with further increasing Eu^{3+} ion concentration due to the concentration quenching (CQ) of Eu^{3+} ion. The chromaticity coordinates of CZSO:Eu^{3+} phosphor with excitation at 395 nm are about (0.5987, 0.4009). The CQ mechanism may explained by the critical distance (R_c) between nearby Eu^{3+} ions, which is calculated by the following formula [11]:

$$R_c = 2\left[\frac{3V}{4\pi xN}\right]^{1/2} \quad (1)$$

where V is the volume of the unit cell, x is the critical doped concentration of Eu^{3+} ion, and N is the number of sites available for the dopant in the unit cell. According to the lattice parameters of host CZSO and the experimental data, $V = 507.60$ Å^3, $N = 2$, and $x = 0.1$. So, R_c value in CZSO:Eu^{3+} can be calculated to be ~ 16.5 Å, which is larger than 5 Å. Figure 3 shows that there is no overlap between PL spectrum of CZSO:Eu^{3+} phosphor with excitation at 395 nm and its PLE spectrum. Thus, the electric multipolar interaction is the main mechanism of CQ in CZSO:Eu^{3+} phosphor.

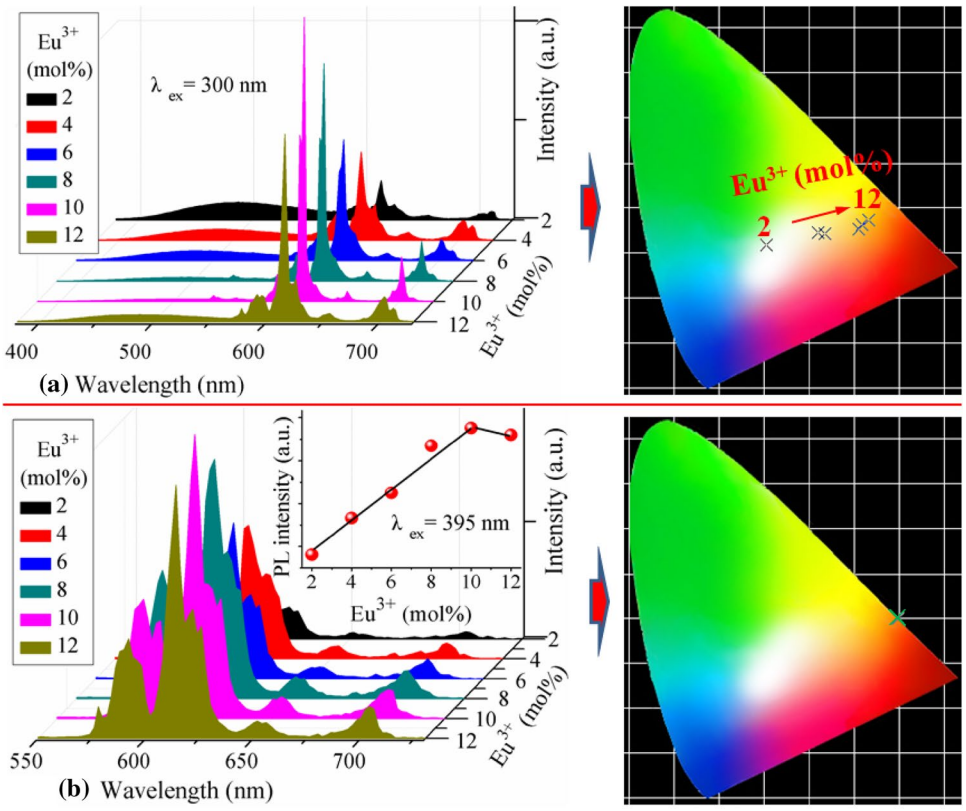

Fig. 5 PL spectra of CZSO:xEu^{3+} (x = 2, 4, 6, 8, 10, and 12 mol%) phosphors at room temperature **a** λ_{ex} = 300 nm and **b** λ_{ex} = 395 nm, and the corresponding CIE chromaticity diagrams and chromaticity coordinates. The inset: The relation between Eu^{3+} ion concentration and PL intensity

Table 1 The chromaticity coordinates of CZSO:xEu^{3+} (x = 2, 4, 6, 8, 10, and 12 mol%) phosphors with excitation at 300 and 395 nm

Eu^{3+} (mol%)	Chromaticity coordinates (x, y)	
	λ_{ex} = 300 nm	λ_{ex} = 395 nm
2	(0.3061, 0.3165)	(0.5987, 0.4009)
4	(0.4204, 0.3445)	
6	(0.4338, 0.3419)	
8	(0.5102, 0.3524)	
10	(0.5177, 0.3625)	
12	(0.5323, 0.3717)	

PL spectra of CZSO:10%Eu^{3+}, yBi^{3+} (y = 2, 4, 6, 8, and 10 mol%) phosphors under 300 nm excitation at room temperature, the corresponding CIE chromaticity diagram and chromaticity coordinates, and the relation between PL intensity and Bi^{3+} concentration are displayed in Fig. 6. PL intensity in the range of 350–570 nm increases with increasing of Bi^{3+} concentration from 2 mol% to 6 mol% owing to the ET among Bi^{3+} ions. PL intensity is the strongest when Bi^{3+} concentration is ~6 mol% and decreases with further increasing Bi^{3+} concentration due to the CQ of Bi^{3+} ions. It can also be observed that PL spectra in the range of 350–570 nm show red-shift due to the emission of Bi^{3+} ion, which is affected by the host crystal field. In host CZSO, there are two Ca sites (Ca(1) and Ca(2)), which are replaced by Bi^{3+} ions. The emission red-shift of Bi^{3+} ion with increasing Bi^{3+} concentration is also observed in other Bi^{3+}-doped materials, such as $ZnWO_4$:Bi^{3+} [11] and $Ca_5(BO_3)_3F$:Bi^{3+} [35]. PL intensity in the range of 570–725 nm increases with increasing of Bi^{3+} concentration from 2 to 6 mol% owing to the ET from Bi^{3+} to Eu^{3+} ions, reaches the maximum when Bi^{3+} concentration is ~6 mol%, and decreases with further increasing Bi^{3+} concentration due to the CQ of Bi^{3+} ions. The experimental result indicates that the optimal Bi^{3+} ion concentration in CZSO:10%Eu^{3+}, Bi^{3+} phosphor is about 6 mol%, and the co-doping Bi^{3+} ion is helpful for the luminescence property improvement of CZSO:Eu^{3+} phosphor. According to the chromaticity diagram, it can also be found that CZSO:10%Eu^{3+}, Bi^{3+} phosphor shows a tunable emission from blue to red light with increasing Bi^{3+} concentration in the range of 2–10 mol% and the corresponding chromaticity coordinates are changed from (0.2296, 0.1351) to (0.3601, 0.2103). that is to say, the co-doping Bi^{3+} ion may be used to adjust the emission color of CZSO:Eu^{3+} phosphor. The similar influence of Bi^{3+} ion to Eu^{3+} ion has been reported in other references [7, 13, 14, 30, 31]. According to host CZSO lattice parameters and experimental data, V = 507.60 Å^3, N = 2, and $x = x_{Eu3+} + x_{Bi3+} = 0.1 + 0.06 = 0.16$. To using the formula (2), R_c value in CZSO:10%Eu^{3+}, Bi^{3+} is calculated to be ~14.5 Å, which is larger than 5 Å. Thus, the electric

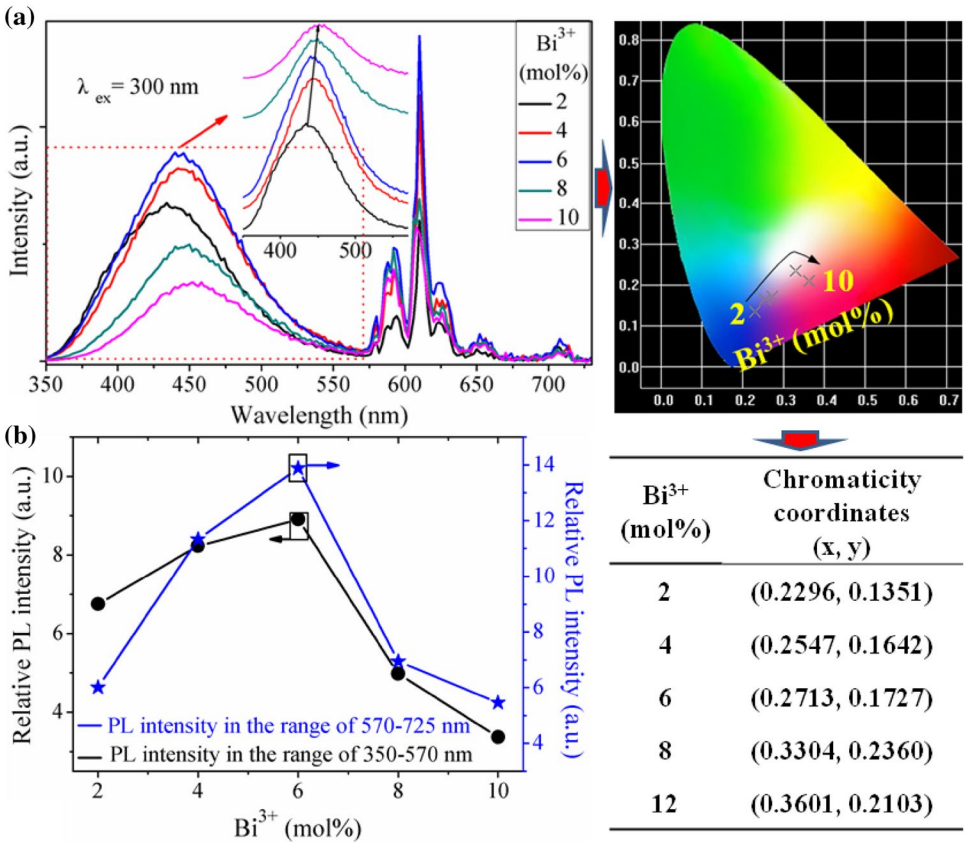

Bi^{3+} (mol%)	Chromaticity coordinates (x, y)
2	(0.2296, 0.1351)
4	(0.2547, 0.1642)
6	(0.2713, 0.1727)
8	(0.3304, 0.2360)
12	(0.3601, 0.2103)

Fig. 6 **a** PL spectra of CZSO:10%Eu^{3+}, yBi^{3+} (y = 2, 4, 6, 8, and 10 mol%) phosphors at room temperature (λ_{ex} = 300 nm) and the corresponding CIE chromaticity diagram and chromaticity coordinates. The inset: PL spectra in the range of 350–570 nm. **b** The relation between PL intensity and Bi^{3+} concentration

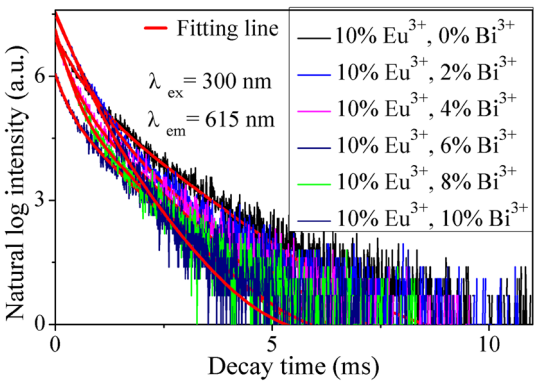

Fig. 7 Decay curves of CZSO:10%Eu^{3+}, yBi^{3+} (y = 2, 4, 6, 8, and 10 mol%) phosphors at room temperature (λ_{ex} = 300 nm and λ_{em} = 615 nm) and the corresponding fitting lines (red line)

multipolar interaction is the main mechanism of CQ in CZSO:10%Eu^{3+}, Bi^{3+} phosphor.

Decay curves of CZSO:10%Eu^{3+}, yBi^{3+} (y = 2, 4, 6, 8, and 10 mol%) phosphors at room temperature and the corresponding fitting lines (red line) are presented Fig. 7. The monitored wavelength is 615 nm with excitation at 300 nm. The decay curves can be well fitted with a double-exponential function [36]:

$$I_{(t)} = I_0 + A_1\exp(-t/\tau_1) + A_2\exp(-t/\tau_2) \quad (2)$$

where I(t) is the luminescence intensity at time t, A_1 and A_2 are the fitting constants, τ_1 and τ_2 are the decay times for the exponential components. Moreover, the effective decay time (τ^*) may be determined by the formula as follows [37]:

$$\tau^* = \left(A_1\tau_1^2 + A_2\tau_2^2\right)/\left(A_1\tau_1 + A_2\tau_2\right) \quad (3)$$

So, the effective decay time (τ^*) values are determined to be 2.68, 2.48, 2.11, 2.08, 1.87, and 1.72 ms for CZSO:10%Eu^{3+}, yBi^{3+} (y = 0, 2, 4, 6, 8, and 10 mol%) phosphors, respectively. The function ($\tau = 1/(k_r + k_i)$, where k_r is the probability of radiative decay and k_i is the probability of nonradiative decay processes from the same state) may be used to describe the experimentally observed decay time [36]. The ET between Eu^{3+} and Bi^{3+} ions results in the increase of k_r. So lifetime decreases with increasing Bi^{3+} concentration.

Generally, the lifetimes may also be used to determinate the ET efficiency by the following formula [38]:

$$\eta_T = 1 - -\left(\tau_s/\tau_{s0}\right) \quad (4)$$

where τ_{s0} value is the lifetime of CZSO:10%Eu^{3+} phosphor, τ_s is the lifetime of CZSO:10%Eu^{3+}, yBi^{3+} (y = 2, 4, 6, 8, and 10 mol%) phosphors, and η_T is the ET efficiency. So, η_T values for CZSO:10%Eu^{3+}, yBi^{3+} may be calculated to be 7.5%, 21.3%, 22.4%, 30.2%, and 35.8%.

4 Conclusions

In summary, we successfully synthesize a series of CZSO:R (R = Eu^{3+}, Bi^{3+}, and Eu^{3+}/Bi^{3+}) phosphors in air through high-temperature solid-state method. The XRD patterns and luminescence properties confirm that all samples have only a pure phase (CZSO). With excitation at 300 nm, host CZSO emits blue light, CZSO:Eu^{3+} and CZSO:Eu^{3+}, Bi^{3+} phosphors can show tunable emission with changing Eu^{3+} or Bi^{3+} concentration. The luminescence properties of host (CZSO), CZSO:Eu^{3+} and CZSO:Eu^{3+}, Bi^{3+} phosphors make clear that ET process from host and Bi^{3+} ion to Eu^{3+} ion can formed. In CZSO:Eu^{3+} phosphor, the optimal Eu^{3+} concentration is ~ 10 mol%. In CZSO:10%Eu^{3+}, Bi^{3+} phosphor, the optimal Bi^{3+} concentration is ~ 6 mol%. The energy level diagrams of Bi^{3+} and Eu^{3+} ions are used to explain the luminous mechanism of CZSO:Eu^{3+}, Bi^{3+} phosphor. The experimental results indicate that the codoping Bi^{3+} ion helpful for the luminescence property improvement of CZSO:Eu^{3+} phosphor.

Acknowledgements This work is financially supported by the National Natural Science Foundation of China (Nos. 51862015 and 21701067), Natural Science Foundation of Jiangxi Province (20171BBB2016016), and National Undergraduate Training Program for Innovation and Entrepreneurship (No. 201810419019).

References

1. J. Xiang, J. Zheng, Z. Zhou, H. Suo, X. Zhao, X. Zhou, N. Zhang, M.S. Molokeev, C. Guo, Chem. Eng. J. **356**, 236–244 (2019)
2. H. Guo, X. Huang, Y. Zeng, J. Alloys Compd. **741**, 300–306 (2018)
3. C. Liao, R. Cao, W. Wang, W. Hu, G. Zheng, Z. Luo, P. Liu, Mater. Res. Bull. **97**, 490–496 (2018)
4. Z. Wu, Z. Zhang, C. Huang, J. Liu, M. Wu, Z. Xia, J. Alloys Compd. **734**, 43–47 (2018)
5. F. Kang, L. Li, J. Han, D. Lei, M. Peng, J. Mater. Chem. C **5**, 390–398 (2017)
6. C. Wang, S. Ye, Q. Zhang, Opt. Mater. **75**, 337–346 (2018)
7. R. Cao, C. Liao, F. Xiao, G. Zheng, W. Hu, Y. Guo, Y. Ye, Dyes. Pigment. **149**, 574–580 (2018)
8. M.P. Saradhi, S. Boudin, U.V. Varadaraju, B. Raveau, J. Solid State Chem. **183**(10), 2496–2500 (2010)
9. L. Sun, H. Guo, J. Liang, B. Li, X. Huang, J. Lumin. **202**, 403–408 (2018)
10. S. Mahlik, M. Amer, P. Boutinaud, J. Phys. Chem. C **120**, 8261–8265 (2016)
11. J. Han, L. Li, M. Peng, B. Huang, F. Pan, F. Kang, L. Li, J. Wang, B. Lei, Chem. Mater. **29**(19), 8412–8424 (2017)
12. R. Cao, G. Quan, Z. Shi, Q. Gou, T. Chen, Z. Hu, Z. Luo, J. Mater. Sci.-Mater. Electron. **29**, 5287–5292 (2018)
13. R. Cao, T. Fu, Y. Cao, S. Jiang, Q. Gou, Z. Chen, P. Liu, J. Mater. Sci.-Mater. Electron. **27**, 3514–3519 (2016)
14. S. Zhang, H. Luo, Z. Mu, J. Li, S. Guo, Z. Li, Q. Wang, F. Wu, J. Alloys Compd. **757**, 423–433 (2018)
15. L.S. Cavalcante, J.C. Sczancoski, J.W.M. Espinosa, V.R. Mastelaro, A. Michalowicz, P.S. Pizani, F.S. De Vicente, M.S. Li, J.A. Varela, E. Longe, J. Alloy. Compd. **471**, 253–258 (2009)
16. R. Yu, M. Yuan, Y. Xiong, J. Li, J. Wang, Opt. Mater. Express. **6**(4), 1049–1055 (2016)
17. S. Colin, B. Dupre, G. Venturini, B. Malaman, C. Gleitzer, J. Solid. State Chem. **102**(1), 242–249 (1993)
18. P. Feng, J. Zhang, C. Wu, X. Liu, Y. Wang, Mater. Chem. Phys. **141**(1), 495–501 (2013)
19. R.D. Shannon, Acta Crystallogr. A **32**, 751–767 (1976)
20. J. Huang, L. Zhou, Z. Wang, Y. Lan, Z. Tong, F. Gong, J. Sun, L. Li, J. Alloys Compd. **487**, L5–L7 (2009)
21. Z.L. Wang, J.C. Zhang, G.S. Zheng, Y.Q. Liu, Y.L. Zhao, J. Lumin. **132**, 2817–2821 (2012)
22. P. Boutinaud, Inorg. Chem. **52**, 6028–6038 (2013)
23. F. Kang, H. Zhang, L. Wondraczek, X. Yang, Y. Zhang, D. Lei, M. Peng, Chem. Mater. **28**(8), 2692–2703 (2016)
24. R. Cao, G. Quan, Z. Shi, Z. Luo, Q. Hu, S. Guo, J. Lumin. **181**, 332–336 (2017)
25. G. Zhou, X. Jiang, J. Zhao, M. Molokeev, Z. Lin, Q. Liu, Z. Xia, ACS Appl. Mater. Interfaces. **10**, 24648–24655 (2018)
26. X. Huang, S. Wang, B. Li, Q. Sun, H. Guo, Opt. Lett. **43**(6), 1307–1310 (2018)
27. M. Jayachandiran, G. Annadurai, S. Masilla Moses Kennedy, J. Lumin. **201**, 196–202 (2018)
28. R. Cao, D. Peng, T. Fu, Z. Luo, S. Zhou, S. Jiang, J. Fu, Synthesis, J. Mater. Sci.-Mater. Electron. **27**(8), 8094–8099 (2016)
29. X. Zhang, Z. Zhu, Z. Sun, Z. Guo, J. Zhang, J. Lumin. **203**, 735–740 (2018)
30. R. Cao, T. Fu, D. Peng, C. Cao, W. Ruan, X. Yu, Synthesis, Spectrochimica Acta Part A **169**, 192–196 (2016)
31. R. Wei, Z. Zheng, Y. Shi, X. Peng, H. Wang, X. Tian, F. Hu, H. Guo, J. Alloys Compd. **767**, 403–408 (2018)
32. H. Yun, S. Kim, S. Park, Opt. Mater. **72**, 571–577 (2017)
33. H.T. Sun, J.J. Zhou, J.R. Qiu, Prog. Mater. Sci. **64**, 1–72 (2014)
34. E. Sreeja, S. Gopi, V. Vidyadharan, P. Remya Mohan, C. Joseph, N.V. Unnikrishnan, P.R. Biju, Powder Technol. **323**, 445–453 (2018)
35. X. Li, P. Li, Z. Wang, S. Liu, Q. Bao, X. Meng, K. Qiu, Y. Li, Z. Li, Z. Yang, Chem. Mater. **29**, 8792–8803 (2017)
36. G. Blasse, B.C. Grabmaier, L. Materials, Springer. Berlin, 1994
37. G. Liu, B. Jacquier, *Spectroscopic Properties of Rare Earths in Optical Materials* (Springer, Berlin, 2005)
38. K. NaveenKumar, L. Vijayalakshmi, J. SuKim, Dyes Pigment. **151**, 403–410 (2018)